Coordination Networks Derived from Pyridyl Functionalized Dipodal Silane Ligands and their Possible Ferroelectric Behaviour

A Thesis

Submitted to

Indian Institute of Science Education and Research Pune

in partial fulfillment of the requirements for the

BS-MS Dual Degree Programme

by

Atul Chaudhary

Indian Institute of Science Education and Research Pune

Dr. Homi Bhabha Road,

Pashan, Pune 411008, INDIA

March 2018

Supervisor: Dr. R. Boomi Shankar

Department of Chemistry

Indian Institute of Science Education and Research, Pune.

Certificate

This is to certify that this dissertation entitled “Coordination Networks Derived from Pyridyl Functionalized Dipodal Silane Ligands and their Possible Ferroelectric Behaviour” for the partial fulfilment of the BS-MS dual degree programme at the Indian Institute of Science Education and Research, Pune represents work carried out by Atul Chaudhary at the Indian Institute of Science Education and Research Pune, under the supervision of Dr. R. Boomi Shankar, Department of Chemistry, during the academic year 2017-2018.

Dr. R. Boomi Shankar

Committee:

Dr. R. Boomi Shankar

Dr. Vaidhyanathan R.

This thesis is dedicated to my Parents & Sister

Declaration

I hereby declare that the matter embodied in the report entitled “Coordination Networks Derived from Pyridyl Functionalized Dipodal Silane Ligands and their Possible Ferroelectric Behaviour” are the results of the work carried out by me at the Department of Chemistry, Indian Institute of Science Education and Research, Pune, under the supervision of Dr. R. Boomi Shankar and the same has not been submitted elsewhere for any other degree.

Atul Chaudhary

Acknowledgement

At first I would like to express my gratitude towards my supervisor Dr. R. Boomi Shankar for accepting me as a project trainee and giving me informative and excellent guidance throughout its execution. I would like to thank him as he had given all the possible opportunities and freedom to pursue research under his guidance. At last, I feel privileged to have worked under his guidance and supervision.

I would like to thank Prof. K. N. Ganesh (former director) and Prof. Jayant B. Udgaonkar (present director) for giving outstanding research facilities, financial support that I have been privileged with, during my research here at Indian Institute of Science of Education and Research (IISER) Pune, India.

I would like to acknowledge my sincere gratitude to Thesis Advisory Committee (TAC) member Dr. Vaidhyanathan R. for his intellectual support, encouragement and valuable suggestions.

I would like to convey my indebtedness to Vijayakanth. T (Ph.D student) for the valuable advices throughout the project and motivating me during the tough times. I would like to thank all the RBS lab members Dr. Anant Kumar Srivastava, Dr. Ashok Yadav, Mahesh S. Deshmukh, Rajasekar, Rishabh, Neetu, Meghamala, Sachin, Swati, Sravan, Prakash, Harsh, Uddipana, Anupriya for their help during the experiments, analysis and for the discussions and care. Finally, I want to thank my friends for their support throughout my project work.

Atul Chaudhary

Abstract

Design and synthesis of 2D Coordination networks derived from pyridyl functionalized dipodal silane ligands for their utility in metal-organic based ferroelectric compounds has been reported. Metal-organic based ferroelectric materials have gained importance in the recent years attributing to their synthetic simplicity with tunable and switchable properties. A variety of cadmium(II) based coordination networks derived from three different types of pyridyl functionalized dipodal silane ligands (L^1, L^2, L^3) were developed that could generate polar non-centrosymmetric space group which is essential for exhibiting ferroelectric behaviour. The crystal structure of Compound **1** was solved in polar non-centrosymmetric space group tetragonal *P4nc*. The compound **1** can sustain its stability upto 473 K without any phase transitions. The ferroelectric measurements on Compound **1** showed the maximum remnant polarization (P_r) value of 0.0162 $\mu C/Cm^2$ and maximum saturation (P_s) polarization value of 0.0152 $\mu C/Cm^2$. The metal-complexes were characterized by single crystal X-ray diffraction, powder X-ray diffraction, IR spectroscopy, melting point analysis, TGA & DTA analysis, ferroelectric measurements.

Contents

1 Introduction

1.1 Brief overview on Coordination Networks……...1

1.2 Brief overview on Ferroelectric Materials……2

1.3 Our Approach……...5

2 Synthesis of Ligands & Coordination Networks

2.1 Experiment Materials & Methods……...7

2.2 Preparation of Bis(3-pyridyl)dimethylsilane (L^1)……....7

2.3 Preparation of Bis(3-pyridyl)diphenylsilane (L^2)……....7

2.4 Preparation of Bis(3-pyridyl)methylphenylsilane (L^3)……....8

2.5 Preparation of Tetrapodal Silane Ligands (L^4).....8

2.6 Preparation of Coordination Networks.....9

3 Result & Discussion

3.1 Characterization of Ligands….....10

3.2 Crystal structure & VT-PXRD studies of L^2.....14

3.3 Crystal structure & VT-PXRD studies of compound **1**.....15

3.4 Crystal structure of compound **2**.....17

3.5 Crystal structure of compound **3**.....17

3.6 Crystal structure of compound **4**.....18

3.7 Crystal structure of compound **5**.....20

3.8 Ferroelectric studies.....22

3.9 Coordination network derived from tetrapodal silane ligand.....25

3.10 Future Aspects.....26

4 **Conclusion**……27

Refrences.....28

List of Figures

1. Design of Coordination Networks in different Dimensions…….....1
2. Illustration of crystallography point groups with ferroelectric, piezoelectric & pyroelectric domains…….....2
3. Polarization (P) versus Electric field (E) hysteresis loop.....3
4. Ferroelectric switching in Co based MOF.....4
5. Ferroelectric metal-organic assemblies supporting Di & tripodal P-N ligands.....5
6. Schematic representation of the overview of work……...6
7. Characterization of L^1…….....11
8. Characterization of L^2…….....12
9. Characterization of L^3.....13
10. Crystal structure of L^2…….....14
11. Variable temperature PXRD studies of L^2 .....…….....15
12. View of two-dimensional network of compound **1**.....16
13. Variable temperature PXRD studies of compound **1**.....16
14. View of two-dimensional network of compound **2**.....17
15. View of one-dimensional network of compound **3** …….....18
16. View of two-dimensional network of compound **4**.....19
17. View of two-dimensional network of compound **5**.....20
18. TGA & DTA Plot for compound **1**…….....21
19. P-E loop at 0.1 Hz at Various Temperatures……22
20. P-E loop with variable frequency at constant temperature of 150^0C……23
21. P-E loop with variable frequency at constant temperature of 175^0C……..24
22. View of three-dimensional network of compound **6**.....26

Chapter 1

Introduction

1.1 Brief overview of Coordination Networks

The field of coordination networks has evolved over a period of time to an extent where its utility in designing multifunctional framework has reached tremendous milestones.[1] An organic ligand (rigid or flexible) plays the role of the linker via coordination with the metal center to yield coordination networks with exciting and fascinating topologies. Due to the type of metal ions and the organic linker ligands these coordination networks form assemblies composed of extended arrays of one, two or three-dimensional architectures (Fig.1). Several of these coordination networks have attracted the interest of many researchers owing to their applications in the areas of adsorption, storage, magnetism, photoluminescence, drug delivery, electric conductivity, heterogeneous catalysis, dielectric and ferroelectric properties.[2]

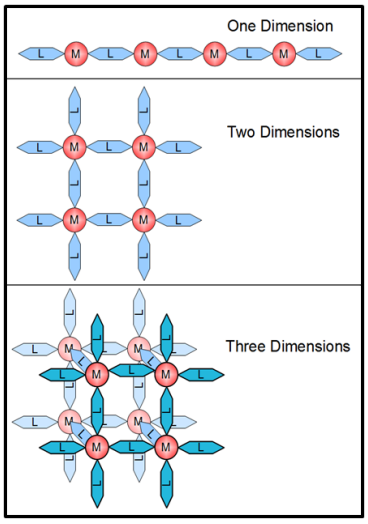

Figure 1: Design of Coordination Networks in Different Dimensions.

Among all these applications, coordination networks possessing dielectric and ferroelectric behavior are far less studied. Preparation of such coordination networks is always a challenging task and is affected by the factors such as core structure of the precursors, temperature, complicated synthetic procedure for organic ligands, yields of the desired network and importantly symmetries of the obtained frameworks. Therefore, in our current research work, we have tried to emphasize on simplification of synthetic procedure for the ligand and metal complexes. Also with the use of main group element “silicon” aids in getting identical ligand topologies for various functional groups with the possibility of obtaining tunable supramolecular assemblies. Recent studies from our group have shown that such approaches offer excellent control on host-guest chemistry, stimuli-responsive luminescent properties,

dielectric and ferroelectric properties for the obtained coordination networks for ligands containing N-donor functionalities.[3] Also, it has been well known that Pd(II) based coordination complexes along with other functional supramolecular materials are found to make macrocyclic rings with N-donor ligands and these macrocycles have an important role to play in the field of molecular recognition, drug delivery, catalyst, biomimics and storage.[4] The N-donor heterocycles functionalized on main-group scaffolds have excellent ability to coordinate with the transition metal ions. Especially, the silicon-containing pyridyl ligands have the excellent adjustable bridging ability and length. Due to its larger size, as compared to the carbon-driven backbone, it has a flexible angle around it with non–rigid conformation and electronic effects of the silicon atom.[5] Owing to these advantages of N-donor functionalized ligands and silicon centric moieties, we set out to explore their utility in obtaining metal-organic materials based on pyridyl-silane ligands and explore their potential for ferroelectric properties.

1.2 Brief overview on Ferroelectric Materials

Ferroelectric materials are the special type of dielectrics whose spontaneous polarization can be reversed on the application of an external electric field. It is a state of matter with a macroscopic reversible static electric dipole expected in an ionic insulator without any inversion symmetry. Ferroelectric compounds should have the space groups belonging to point groups of the type C_1, C_s, C_2, C_{2V}, C_3, C_{3V}, C_4, C_{4V}, C_6 and C_{6V} (Fig.2).

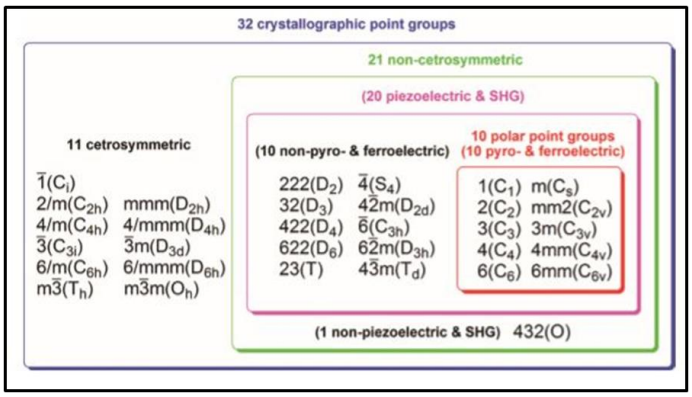

Figure 2: Illustration of crystallographic point groups with the classification of ferroelectric, piezoelectric, pyroelectric domains.

These compounds on the application of external electric field exhibit P-E hysteresis loop (Fig.3). These materials attain saturation polarization (P_S) on increasing the electric field. When the strength of electric field is traced back to zero, these materials retain some polarization known as remnant polarization (P_r). However, upon reversal of the electric field strength from zero leads to the generation of opposite polarization vector which is formally known as switching.

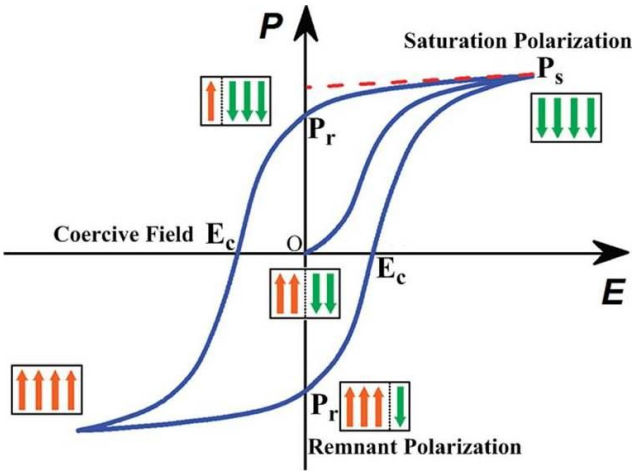

Figure 3: Polarization (P) versus Electric field (E) hysteresis loop. (Adapted from "Xiong et al. Chem. Rev. **2012**, 112, 1163" © 2012 American Chemical Society.)

Ferroelectrics exhibit properties of piezoelectrics and pyroelectric because of the presence of polarization due to mechanical stress or temperature change. In the recent years, materials having ferroelectric, magnetoelectric and multiferroic properties have attracted the interest of many researchers due to their extensive applications in various classes of operational devices. They are widely used in ferroelectric random access memories, data storage, energy harvesters, infra-red detectors, piezoelectric and fire sensors, ferroelectric capacitors, non-linear optoelectronic devices, etc. They have various applications in ferroelectric field effect transistors, non-volatile memory storage, radio frequency identification cards, thermoresistors, oscillators, filters, medical ultrasound devices, light deflectors, transpolarizers, modulators and displays.[6-12] The commercially available ferroelectric materials include barium titanate (BTO) and lead titanate. But these ferroelectric materials deal with certain drawbacks such as the need of harsh conditions for synthesis, heavy metals with high toxicity and economic issues. Due to all these limitations, there is a need for some alternate source which can replace these traditionally used commercial ferroelectric materials. A wide variety of new materials such as inorganic-organic hybrid, pure oxide compounds and polymers have been examined for ferroelectric properties .[13- 19]

The metal-organic ferroelectric materials have gained much attention because of their simplified synthetic procedure, comparatively softer conditions for fabrications, flexibility and light metal content with low toxicity.[20] The first ferroelectric material, Rochelle salt, also belongs to the class of metal-organic materials.[21] It consists of tartrate anion (organic scaffold) and K^+ and Na^+ cations (inorganic scaffold). The advantage of incorporating inorganic-organic hybrid for exhibiting ferroelectricity is determined by the fact of inducing flexibility, tunability as well as simplified synthesis and structural variations in metal-organic materials. Further, the ferroelectric

properties have been explored in a variety of metal-organic systems such as metal-organic sulfates, metal-amino acid systems, metal-propionates, metal formates, and organo-halogenometallates. The polar metal-formate frameworks have been extensively studied for their ferroelectric and multiferroic behaviour. They exhibit a three-dimensional perovskite lattice (ABX_3) in which the ordering of the organic cation within the cavity of the anionic metal-formate framework is responsible for the ferroelectricity. Ferroelectricity has also been discovered in other metal-organic salts that adopt perovskite structure such as methylammonium lead halides, pyrrolidinium manganese halide, organo-halogenometallates. A recently discovered 3-dimensional molecular ferroelectric perovskite [(3-ammoniopyrrolidinium)$RbBr_3$], with T_c (440 K) and very high thermal stability, exhibits multiaxial polarization which is rare in 3D metal-organic perovskites.[22] Further, the scope of structural engineering or tailoring in such ferroelectric metal-organic systems provides the opportunity to induce additional properties (such as non-linear optical behaviour, high dielectric constant, photoluminescence, magnetism) that can be utilized to develop high-performance devices like ferroelectric fluorescent displays, optoelectronic devices, and magneto-optoelectronic systems.[23-25]

Apart from these materials, ferroelectricity has also been revealed in polar metal-organic frameworks (MOFs). Mak and co-workers have synthesized a Co(II) based homochiral metal-organic framework constructed by (1,3-dicarboxy-5-benzyl)carboxymethyl glycine and 1,3-bis(4-pyridyl)ethane ligands that contain helical water columns which leads to the solvation (on) and desolvation (off) assisted ferroelectric switching (Fig.4). Various strategies have been utilized to achieve non-centrosymmetric geometries in MOFs such as involving chiral linkers, polar guests, non-coordinating polar linkers and building blocks exhibiting three-fold symmetry. Such techniques can be utilized to propose various novel ferroelectric metal-organic materials with interesting polarization attributes.

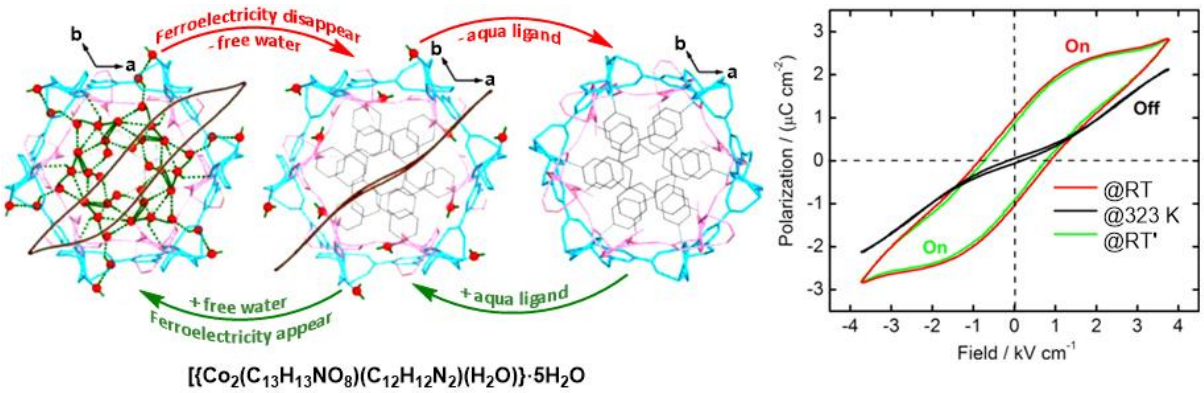

Figure 4: Ferroelectric Switching in Co based MOF due to solvation and desolvation of water molecules. Adapted from "Mak et al. *J. Am. Chem. Soc.* **2013**, *135*, 10214" © 2013 American Chemical Society.

1.3 Our Approach

Earlier efforts from our group involve the utilization of various P-N scaffolds to generate polar ordered materials with potential ferroelectric properties. Thus, pyridyl functionalized di- and tripodal phosphoramide ligands (which favours axially symmetric moieties) have been employed to specifically obtain metal-organic assemblies in discrete (cages and cavitands) structures, 1D-helical and 2D-layered networks in polar point groups. While the polarization in the helical 1D-assemblies were found to originate from the subtle variations in the packing arrangement of the anions, electric polarization in 2D-assembly was governed by the interaction of the solvate molecules with the anions and the host framework. Interestingly, discrete tetrameric cavitands based on the dipodal ligand showed tuned ferroelectric responses by the presence of various hydrated alkali metal guest cations. We have also observed ferroelectric behaviour in M_6L_8 type metal organic cages derived from a C_3-symmetric phosphoric triamide ligand. In all these instances, the tetrahedral symmetry at the phosphorus centre coupled with its asymmetric substitution leads to the formation of either pseudo-C2 symmetric or C3-symmetric ligand backbone which resulted in the formation of axially symmetry assemblies with potential ferroelectric properties (Figure 5).

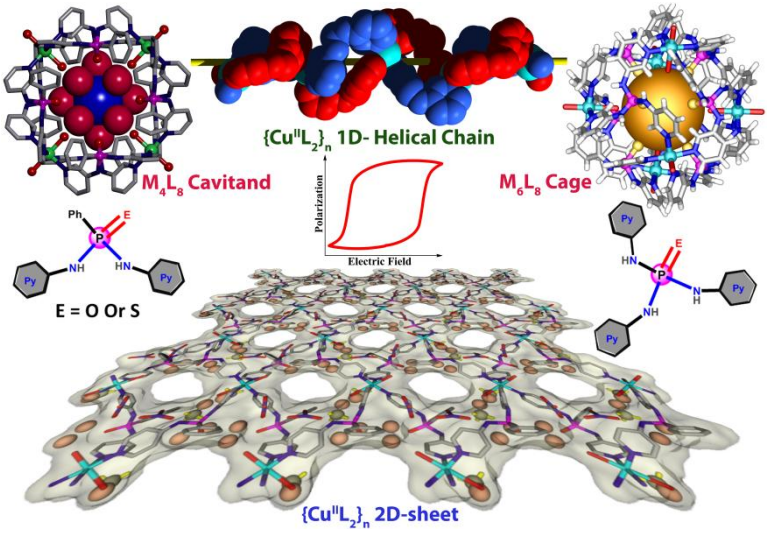

Figure 5: Ferroelectric metal-organic assemblies supported by di- and tripodal P-N ligands.

Inspired by this, we set out to explore the role of other families of tetrahedral ligands containing pyridyl functionalities that support metal-organic materials with noncentrosymmetric crystal parameters. In this regard, tetravalent silicon is an exciting prospect wherein it is possible to tailor its backbone in a simple and systematic way to generate the C2 and C3-symmetric ligand platforms. Herein, we present our efforts to generate new examples of dipodal silane ligands containing pyridyl moieties and some of their metal complexes (Figure 6). Thus, we were able to generate three ligands (L^1, L^2, L^3) which offer such pseudo-C2 symmetric backbone and interesting examples of metal complexes with both centrosymmetric

and noncentrosymmetric structures. Notably, one of the metal complexes that crystallizes in a polar space group tetragonal *P4nc* was found exhibit a ferroelectric response in the polarization versus external electric field (P-E) hysteresis loop measurements.

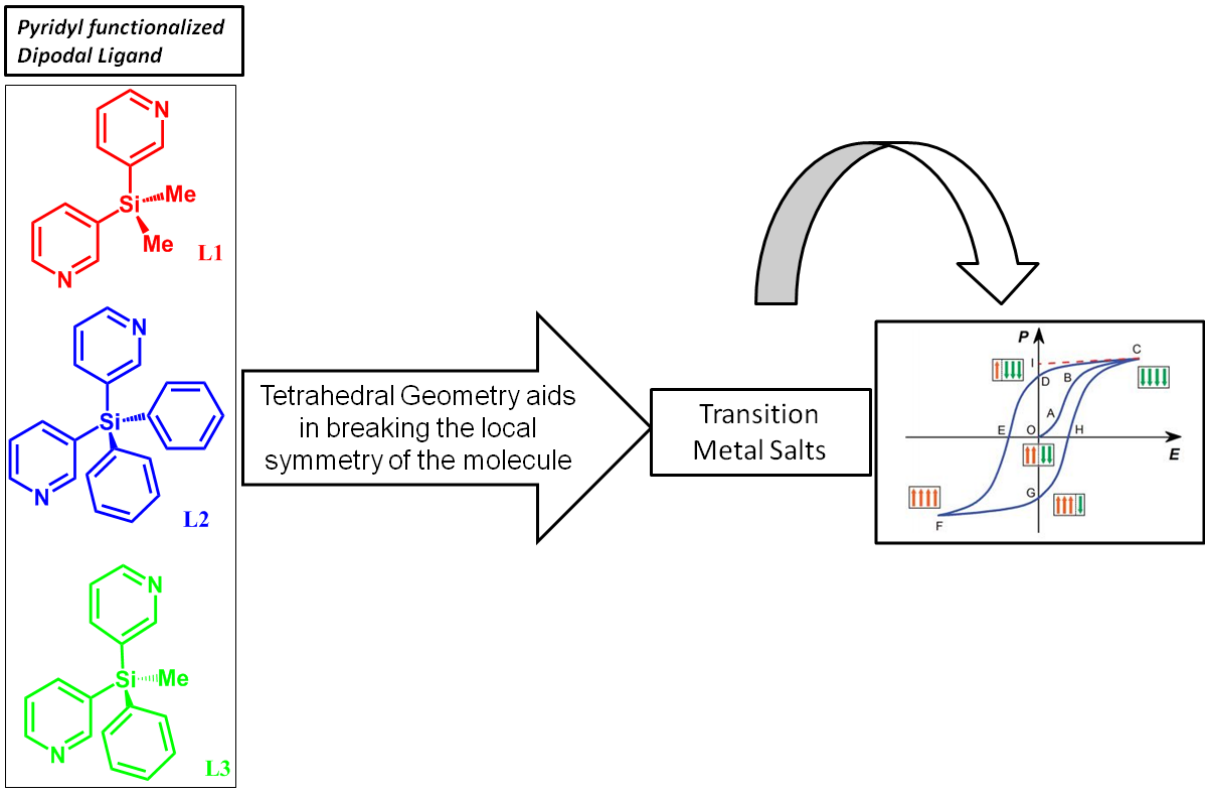

Figure 6: Schematic representation of an overview of work.

Chapter 2

Synthesis of Ligands & Coordination Networks

2.1 Experimental Materials

All manipulations were performed under a dry atmosphere in standard Schlenk glassware. All chemicals used for synthesis were purchased from Sigma-Aldrich and used as received. TLC analysis was performed on aluminum plates with silica gel 60 F_{254}; Column chromatography was carried out on 200-300 mesh silica gel. ^{1}H, ^{29}Si NMR spectra were recorded on Bruker Advanced 400 MHz DPX spectrometer using 1,1,1,1-tetramethylsilane (TMS) as an internal standard. High-resolution mass spectrometry (HRMS) measurements were carried out on a Bruker Impact HD ESI-Q TOF mass spectrometer. The MALDI-TOF/TOF spectra were obtained on an Applied Biosystems spectrometer. The FT-IR spectra were obtained on a PerkinElmer spectrophotometer. Thermogravimetric analysis (TGA) were carried out on Perkin-Elmer STA 6000, TGA analyzer under N_2 atmosphere with a heating rate of 10° C/min. Ferroelectric measurements were obtained on the aixACCT piezoelectric evaluation system.

2.2 Preparation of Bis(3-pyridyl)dimethylsilane (L^1)

A solution of 3-bromopyridine (0.67 ml, 7 mmol) was prepared in dry diethyl ether (30 mL) as a solvent, followed by the dropwise addition of n-Butyl lithium (7.1 mmol, 2.5 M solution in hexane) at -10°C. The reaction mixture was stirred for 1 hour which led to the formation of the yellow suspension. To this yellow suspension, dichlorodimethylsilane (0.38 ml 3.2 mmol) was added at -10°C under nitrogen atmosphere. The temperature of the reaction mixture was brought back to room temperature and under this condition, the reaction mixture was stirred for 12 hours. To this reaction mixture, distilled water (30 ml) was added and then the organic phase was separated from the aqueous phase in the separating funnel. The organic solution was washed with brine solution and dried over Na_2SO_4 which led to the formation of the crude product. The crude product was purified by column chromatography using 60% ethyl acetate in hexane to give L^1 ($C_{12}H_{14}N_2Si$) as a pale yellow solid (62% yield). ^{1}H NMR ($CDCl_3$, $SiMe_4$, ppm): 8.67 (m, 2H), 8.59 (q, 2H), 7.74 (dt, 2H), 7.25 (m, 2H), 0.60 (s, 6H). ^{29}Si NMR ($CDCl_3$, $SiMe_4$, ppm): -8.39.

2.3 Preparation of Bis(3-pyridyl)diphenylsilane (L^2)

A solution of 3-bromopyridine (0.67 ml, 7 mmol) was prepared in dry diethyl ether (30 mL) followed by the dropwise addition of n-Butyl lithium (7.1 mmol, 2.5 M solution in hexane) at -10°C. The reaction mixture was stirred for 1 hour which led to the formation of the yellow suspension. To this yellow suspension,

dichlorodiphenylsilane (0.67 ml 3.2 mmol) was added at -10°C under nitrogen atmosphere. The temperature of the reaction mixture was brought back to room temperature and under this condition, the reaction mixture was stirred for 12 hours. To this reaction mixture, distilled water (30 ml) was added and then the organic phase was separated from the aqueous phase in the separating funnel. The organic solution was washed with brine solution and dried over Na_2SO_4 which led to the formation of the crude product. The crude product was purified by column chromatography on silica gel using 80% ethyl acetate in hexane to give L^2 ($C_{22}H_{18}N_2Si$) as a pale yellow solid (65% yield). ^{1}H NMR ($CDCl_3$, $SiMe_4$, ppm): 8.75 (t, 2H), 8.70 (dd, 2H), 7.85 (dt, 2H), 7.55-7.57 (m, 4H), 7.48-7.52 (m, 2H), 7.42-7.48 (m, 6H), ^{29}Si NMR ($CDCl_3$, $SiMe_4$, ppm): -10.18.

2.4 Preparation of Bis(3-pyridyl)methylphenylsilane (L^3)

A solution of 3-bromopyridine (0.67 ml, 7 mmol) was prepared in dry diethyl ether (30 mL) followed by the dropwise addition of n-Butyl lithium (7.1 mmol, 2.5 M solution in hexane) at -10°C. The reaction mixture was stirred for 1 hour which led to the formation of the yellow suspension. To this yellow suspension, dichloromethylphenylsilane (0.52 ml 3.2 mmol) was added at -10°C under nitrogen atmosphere. The temperature of the reaction mixture was brought back to room temperature and under this condition, the reaction mixture was stirred for 12 hours. To this reaction mixture, distilled water (30 ml) was added and then the organic phase was separated from the aqueous phase in the separating funnel. The organic solution was washed with brine solution and dried over Na_2SO_4 which led to the formation of the crude product. The crude product was purified by column chromatography using 70% ethyl acetate in hexane to give L^3 ($C_{17}H_{16}N_2Si$) as a pale yellow solid (60% yield). ^{1}H NMR ($CDCl_3$, $SiMe_4$, ppm): 8.70 (q, 2H), 8.65 (dd, 2H), 7.77 (dt, 2H), 7.52-7.49 (m, 2H), 7.46-7.38(m, 3H), 7.32-7.28 (m, 2H), 0.92 (s, 3H) ^{29}Si NMR ($CDCl_3$, $SiMe_4$, ppm): -9.16.

2.5 Preparation of Tetrapodal Silane Ligand (L^4)

A solution of 3-Bromopyridine (14.13 ml, 5.84 mmol) in triethylamine (10 ml) as a solvent was prepared. To this solution, tetravinylsilane (2 ml, 0.73 mmol) was added under nitrogen atmosphere. Under this inert condition, tetrakis(triphenylphosphine)palladium(0) (10 mg) as a catalyst was added and the reaction mixture was stirred at 120^{0}C for 48hrs. The reaction mixture was brought back to the room temperature and distilled water (50 ml) was added and then the organic phase was separated from the aqueous phase in the separating funnel. The organic solution was washed with brine solution and dried over Na_2SO_4 which led to the formation of crude product. The crude product was purified by column chromatography using 50% ethyl acetate in hexane to give L^4 (65% yield).

2.6 Synthesis of Coordination Networks

Compound 1 [$C_{26}H_{28}CdN_4O_6Si$]:

Methanolic solution of L^1 (10 mg, 0.04 mmol) was prepared, followed by the addition of aqueous solution of $Cd(NO_3)_2.4H_2O$ (14.39 mg, 0.04 mmol). The resulting solution was filtered through a layer of celite. It was kept for crystallization for 72 hrs which resulted in the formation of white crystals.

Compound 2 [$C_{24}H_{28}CdCl_2N_4Si_2$]:

Methanolic solution of L^1 (10 mg, 0.04 mmol) was prepared, followed by the addition of aqueous solution of $CdCl_2.H_2O$ (9.39 mg, 0.04 mmol). The resulting solution was filtered through a layer of celite. It was kept for crystallization for 72 hrs which resulted in the formation of white crystals.

Compound 3 [$C_{22}H_{18}CdN_4O_6Si$]:

A solution of L^2 (10 mg, 0.04 mmol) in ethyl acetate (3 mL) was prepared, followed by the addition of $Cd(NO_3)_2.4H_2O$ (9.12 mg, 0.04 mmol) in acetonitrile (3 mL). The resulting solution was filtered through a layer of celite. It was kept for crystallization for 72 hrs which resulted in the formation of white crystals.

Compound 4 [$C_{24}H_{20}CdN_4O_6Si$]:

Methanolic solution of L^3 (10 mg, 0.04 mmol) was prepared, followed by the addition of aqueous solution of $Cd(NO_3)_2.4H_2O$ (11.13 mg, 0.04 mmol). The resulting solution was filtered through a layer of celite. It was kept for crystallization for 72 hrs which resulted in the formation of white crystals.

Compound 5 [$C_{26}H_{28}CoN_6S_2Si_2$]:

Aqueous solution of $Co(SCN)_2$ (4.08 mg, 0.02 mmol) was prepared and kept in a 10 cm long layering tube. Methanolic solution of L^1 (10 mg, 0.04 mmol) was slowly added to this layering tube. The layered solutions in the tube were kept for crystallization for 2 days to get pink colored crystals.[26]

Compound 6 [$C_{56}H_{44}Zn\ N_4O_8Si$]:

For the synthesis of compound **6**, we took tetrakis(3-pyridyl)vinylsilane (10 mg, methanol), 2,2′- bipyridyl-4,4′-dicarboxylic acid (10.7mg, DMF) in a screw-capped vial and treated this with $Zn(NO_3)_2.6H_2O$ (13.16 mg, methanol) under solvothermal conditions at 90°C for 36 h & on slowly cooling led to the formation of this 3D coordination network compound **6**.

Chapter 3

Results & Discussions

3.1 Characterization of Ligands:

The silane ligands L^1 - L^3 were synthesized by a two-step reaction in diethylether in which the corresponding diorganodichlorosilanes were first treated with n-BuLi followed by the treatment of 3-bromopyridine (Scheme 1). The purified ligands gave a single peak in their ^{29}Si-NMR spectrum with chemical shifts in the range of -8 to -10 ppm which are consistent with previously reported tetraorganosilane compounds. The ^{1}H-NMR spectra showed signals due to pyridyl and phenyl (and/or methyl) protons. All the ligands gave prominent signals in the mass-spectra due to their parent ions.

Scheme 1:

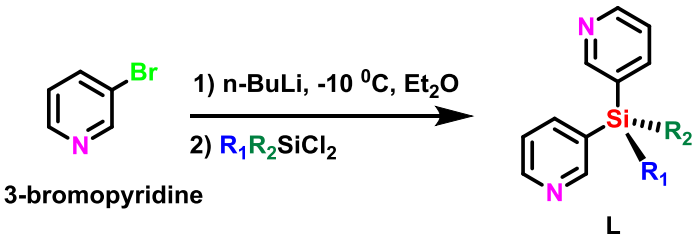

3-bromopyridine

L

Ligand (L)	R_1	R_2
L^1	Me	Me
L^2	Ph	Ph
L^3	Ph	Me

For L^1 the ^{29}Si-NMR gave a single prominent peak around the region -8.39 ppm (Fig.7a). Similarly, the total number of protons for L^1 was in agreement with the observed ^{1}H NMR spectra with six methyl protons at 0.61 ppm and eight pyridyl protons in the region of 7.26 ppm - 8.67 ppm (Fig.7c). The high-resolution ESI-MS spectrum of L^1 gave a sharp peak at m/z = 215.0978 for the parent ion (Fig.7b).

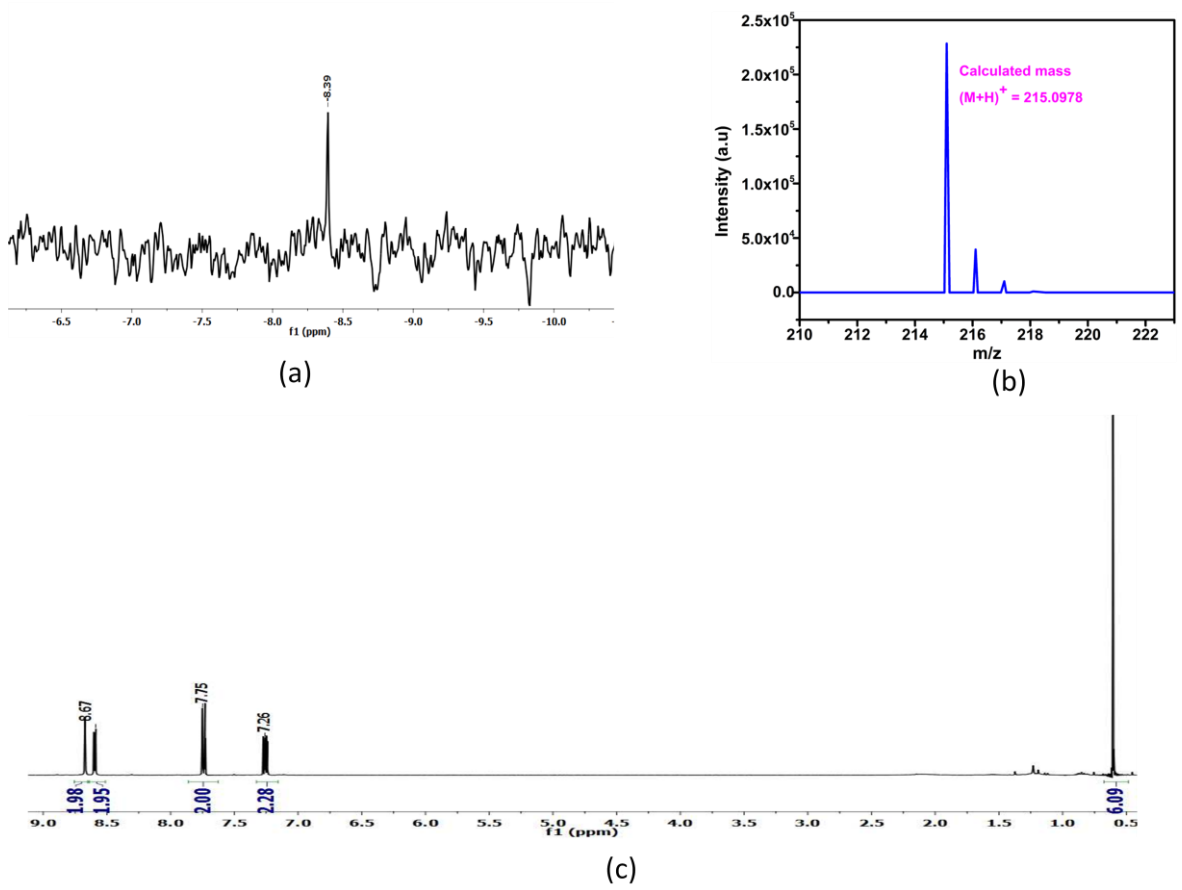

Figure 7: (a) ^{29}Si NMR of L^1**,** (b) High-resolution mass spectrometry spectra of L^1**,** (c) ^{1}H NMR of L^1.

A couple of more dipodal silane ligands analogous to L^1 were prepared (L^2 & L^3) to study the selectivity of the ligand in attaining a coordination network with polar- non-centrosymmetric space group. In L^2, both R_1 & R_2 were replaced by phenyl groups whereas in L^3; only the R_1 group was substituted by phenyl group.

For L^2, the ^{29}Si-NMR gave a single prominent peak around the region -10.18 ppm (Fig.8a). The observed peak for the silicon atom is more deshielded as compared to L^1 due to the electron withdrawing ability of the two phenyl groups. Similarly, the total number of protons for L^2 was in agreement with the observed ^{1}H NMR spectra (Fig.8c). Further, the high-resolution mass spectrometry of L^2 gave the m/z value of 339.1317 which is the respective mass of parent ion (Fig.8b).

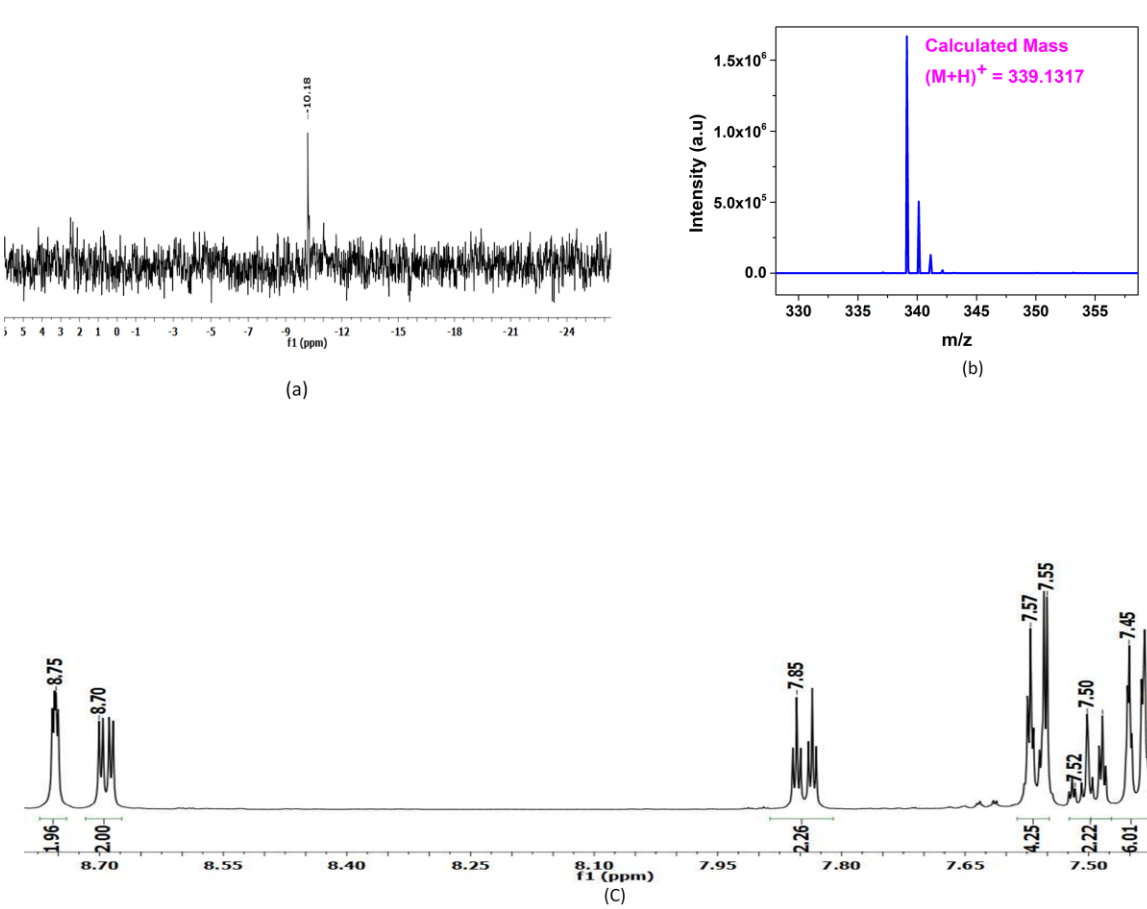

Figure 8: (a) ^{29}Si NMR of L^2, (b) High-resolution mass spectrometry spectra of L^2**,** (c) ^{1}H NMR of L^2

Similarly, for L^3, it was observed that the ^{29}Si-NMR gave a single prominent peak at -9.16 ppm (Fig.9a). A total of sixteen protons were clearly observed in the ^{1}H NMR spectra of L^3 (Fig.9b). The high-resolution mass spectrometry of L^3 gave the m/z value of 277.4218 which is due to the parent ion (Fig.9c). In order to explore the ability of L^2 & L^3 in favoring the formation of non-centrosymmetric molecule, we treated them with cadmium based metal-salts. However, coordination network derived from both L^2 & L^3 resulted in the formation of centrosymmetric coordination networks.

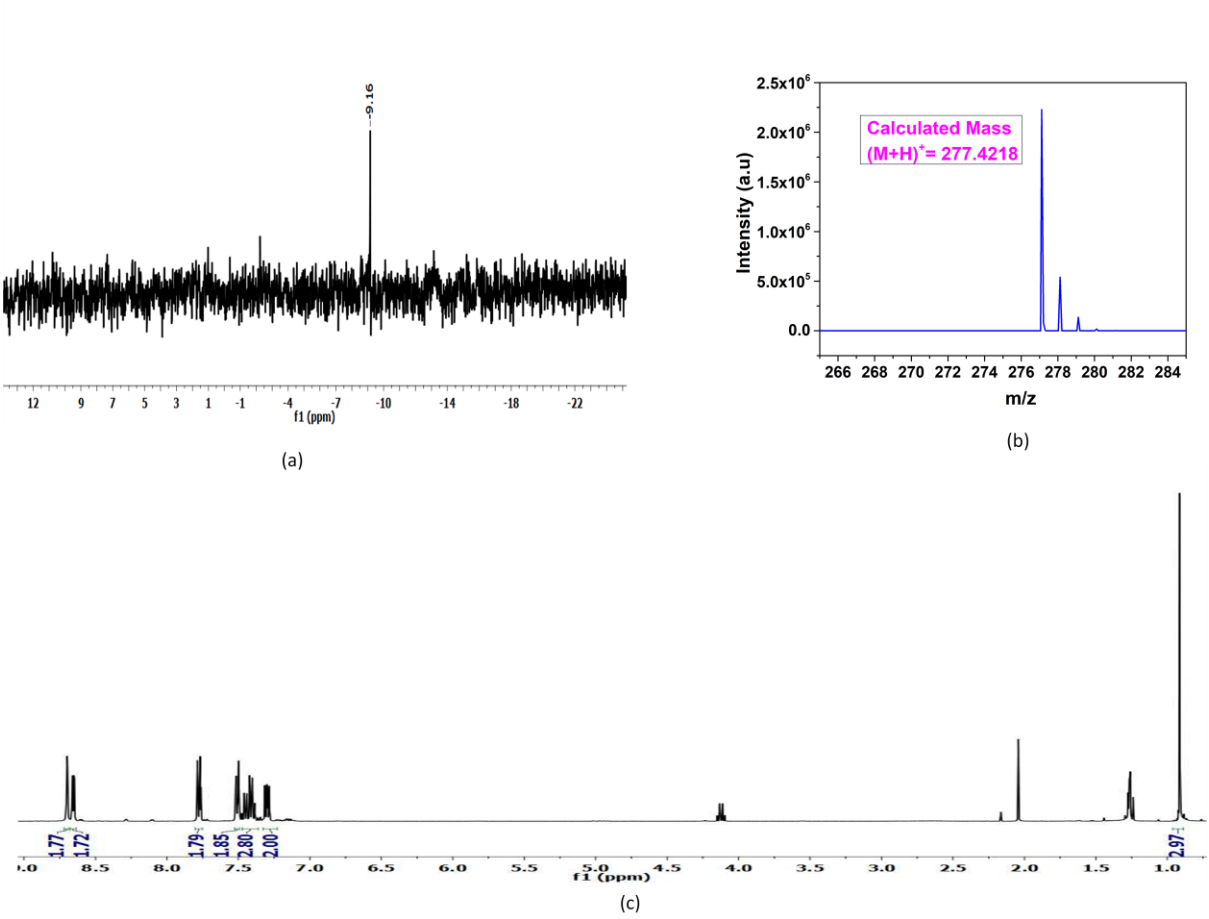

Figure 9: (a) ^{29}Si NMR of **L^3,** (b) High-resolution mass spectrometry Spectra of **L^3,** (c) ^{1}H NMR of **L^3.**

In the end, we got two polar non-centrosymmetric molecules derived from L^1 with transition metal-salts. Both L^2 & L^3 have so far resulted in the formation of centrosymmetric molecules with the same metal-salts. It is very difficult to precisely report the reason for attaining asymmetry in the core structure as it is a consolidated effect of ligand, metal-ion, counter-anion and solvent systems. However, in our study it can be said that apart from the additional role of metal-ion, counter-anion, solvent systems to get non-centrosymmetric frameworks, the ligand backbone also plays a very important role in designing the ferroelectric molecules.

Metal complexes, Crystal Structures & X-ray Diffraction Studies

3.2 Crystal Structure & Variable-Temperature PXRD studies of L^2

We were able to get suitable crystals for single-crystal X-ray analysis for one of the ligands, L^2 (Fig.10). The crystal structure for L^2 was solved in the non-polar non-centrosymmetric space group *P-42$_1$c* with point group "42m" and point group symmetry "D_{2d}" at 150K which was ferroelectric inactive. The bond length between Si atom and carbon atom of the phenyl group is 1.87 Å. To study any further modification in the structural properties (if possible) of L^2 from non-polar non-centrosymmetric space group to polar non-centrosymmetric space, we performed variable temperature powder X-ray diffraction (Fig.11). However, we observed that there is no phase transition in the structure of L^2 even at higher temperatures upto 473 K. The observation of small peak shift in the VT-PXRD of L^2 may be due to the evaporation of crystallized solvate molecules. The Variable temperature PXRD data of L^2 shows distinct fine peaks which are in good match with the simulated peaks derived from the single-crystal X-ray data.

The pyridyl functionalized dipodal silane ligands (L^1) with flexible tetrahedral geometry around the silicon atom has a very good coordinating and bridging ability with the transition metal salts. In literature, these kinds of dipodal silane ligands are extensively used for obtaining coordination complexes with non-rigid conformation exhibiting multifunctional behavior. Thus, these new silane ligands can be used as a flexible platform with the view of obtaining coordination complexes with non-centrosymmetric space groups that can potentially exhibit ferroelectric behaviour.

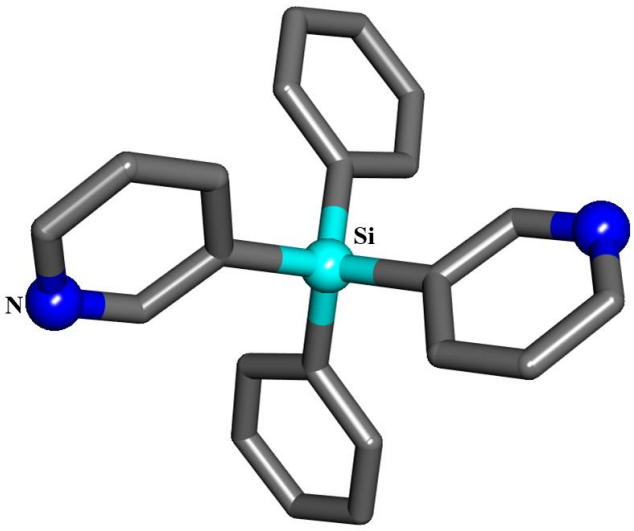

Figure 10: Crystal Structure of L^2**.**

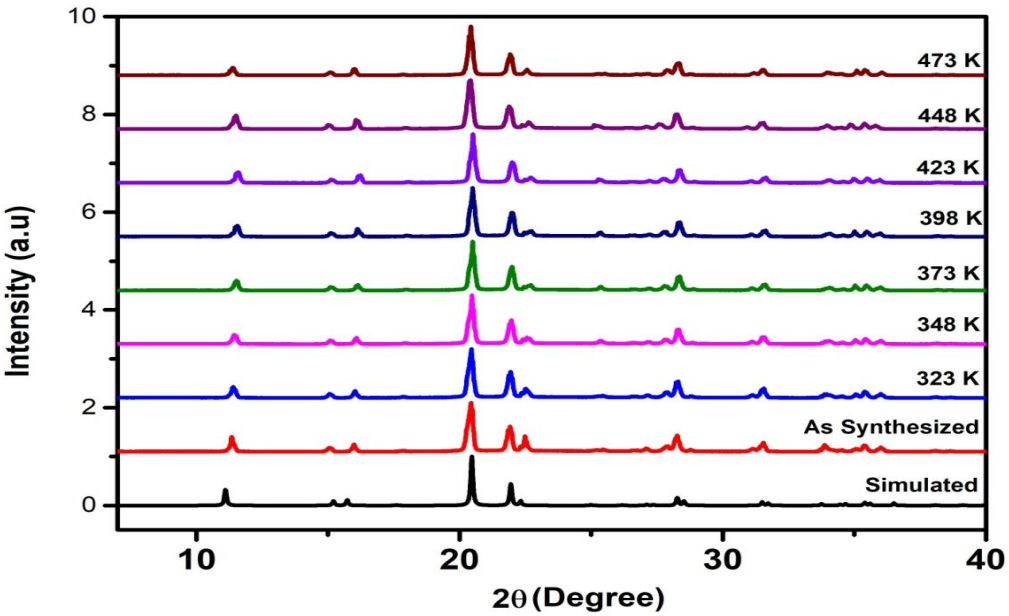

Figure 11: Variable-temperature PXRD pattern of L^2.

3.3 Crystal Structure & Variable-Temperature PXRD studies of Compound 1

Treatment of L^1 with $Cd(NO_3)_2.4H_2O$ gave the compound **1** of formula $[C_{26}H_{28}CdN_4O_6Si]$. The compound **1** is a two-dimensional coordination network (Fig.12) and its crystal structure was solved in tetragonal non-centrosymmetric space group *P4nc* with point group "4mm" and point group symmetry "C_{4v}". The asymmetric unit of compound **1** consists of one Cadmium metal ion with unit occupancy. Each metal-center has an octahedral geometry in which four positions were occupied with nitrogen atoms of the four different pyridyl groups, and the other two positions are coordinated with oxygen atoms of the nitrate anions for charge balance. However, one of the two nitrate ions at of each alternate Cd(II) centres is attached in a gem-bidentate fashion which results in a somewhat skew-trapezoidal geometry at the metal centre. The average bond lengths between Cd(II) ion and nitrogen atom of pyridyl group is 2.3 Å whereas the average bond distances between Cd(II) and oxygen atom of nitrate anion is 2.5 Å. Variable temperature powder X-ray diffraction analysis of compound **1** was performed; it closely resembles with as synthesized phase and their calculated experimental simulated PXRD patterns (Fig.13). No significant order to disorder phase transition was observed in between 298 K to 473 K. As this compound crystallized in polar non-centrosymmetric space group *P4nc* with no change in any phase transition up to 473 K, so we performed ferroelectric measurements on compound **1** from room temperature to 473 K.

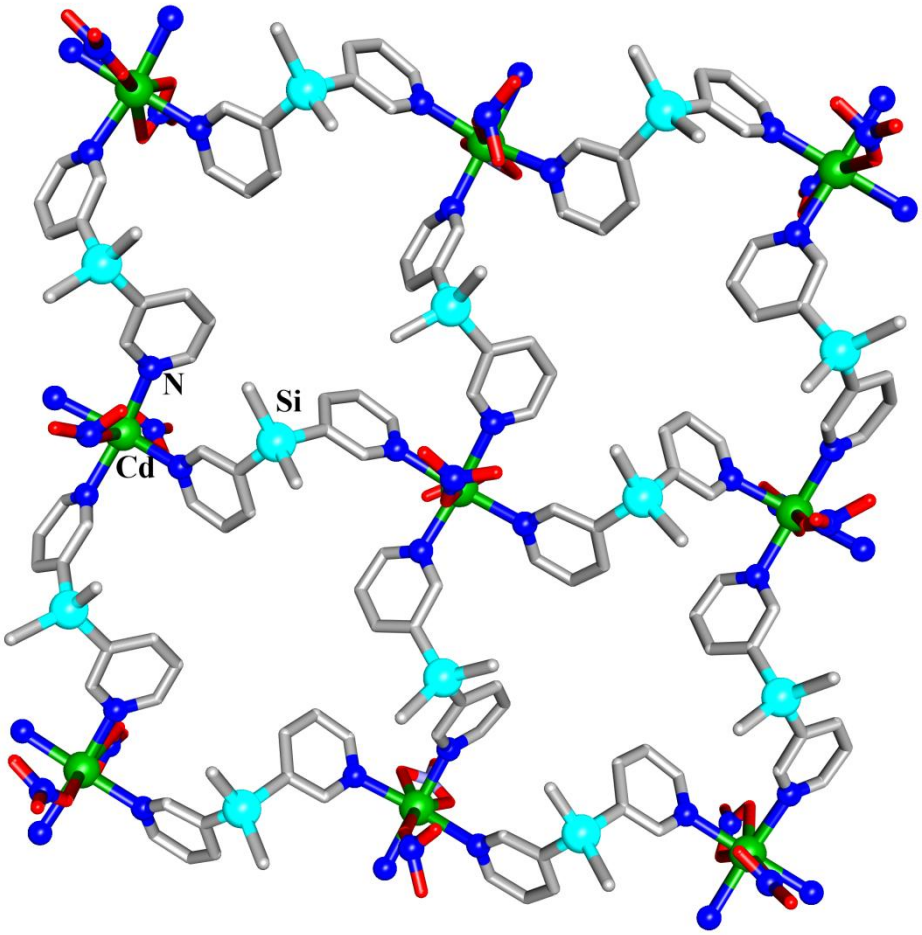

Figure 12: View of two-dimensional network of compound **1**.

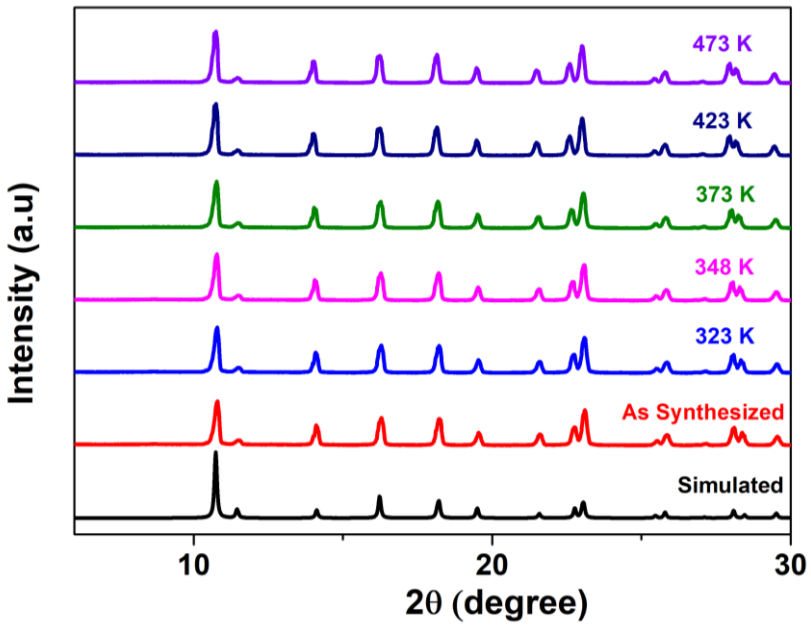

Figure 13: Variable temperature PXRD pattern for compound **1**.

3.4 Crystal Structure of Compound 2

Treatment of L^1 with $CdCl_2.H_2O$ gave rise to a new two-dimensional assembly of formula $[C_{24}H_{28}CdCl_2N_4Si_2]$. The crystal structure of compound **2** was solved in monoclinic centrosymmetric space group *$P2_1/n$* with point group "2/m" and point group symmetry "C_{2h}". A combination of 1:1 metal to ligand ratio was involved to drive the formation of this kind of assembly which attributes to the formation of two-dimensional frameworks (Fig.14). The asymmetric unit of compound **2** consists of one cadmium metal ion with half occupancy. Each metal-center has an octahedral geometry in which it is connected to nitrogen atom of the pyridyl groups and the remaining two *trans*-positions are occupied by chloride ions for charge balance. The bond length between Cd(II) ion and nitrogen atom of pyridyl group is 2.37 Å (average) whereas the bond distance between Cd(II) and chloride atom is 2.60 Å (average).

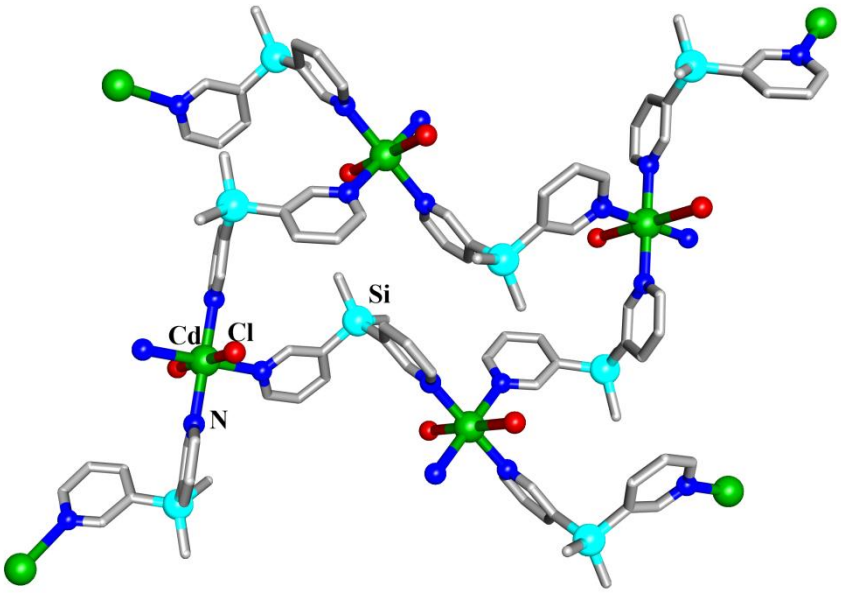

Figure 14: View of two-dimensional network of compound **2**.

3.5 Crystal Structure of Compound 3

Treatment of L^2 with $Cd(NO_3)_2.4H_2O$ gave the compound **3** of formula $[C_{22}H_{18}CdN_4O_6Si]$. The crystal structure of compound **3** was solved in triclinic centrosymmetric space group *P-1* with point group "-1" and point group symmetry "C_i". It exhibits a one-dimensional framework (Fig.15) in which each metal-center has an octahedral geometry in which it is connected to two pyridyl groups through a nitrogen atom and another four positions are coordinated to oxygen atoms of the nitrate anions. The asymmetric unit of compound **3** contains one Cadmium metal ion with unit occupancy. The oxygen atom of the nitrate anion is acting as a bridging

motif to connect two Cadmium metal centers. The bond length between Cd(II) ion and nitrogen atom of pyridyl group is 2.32 Å (average) whereas the bond distance between Cd(II) and oxygen atom of nitrate anion is 2.35 Å (average). Utilizing L^2 for designing coordination networks in 1:1 metal to ligand assemblies resulted in the formation of centro-symmetric structures which were not used for ferroelectric measurements.

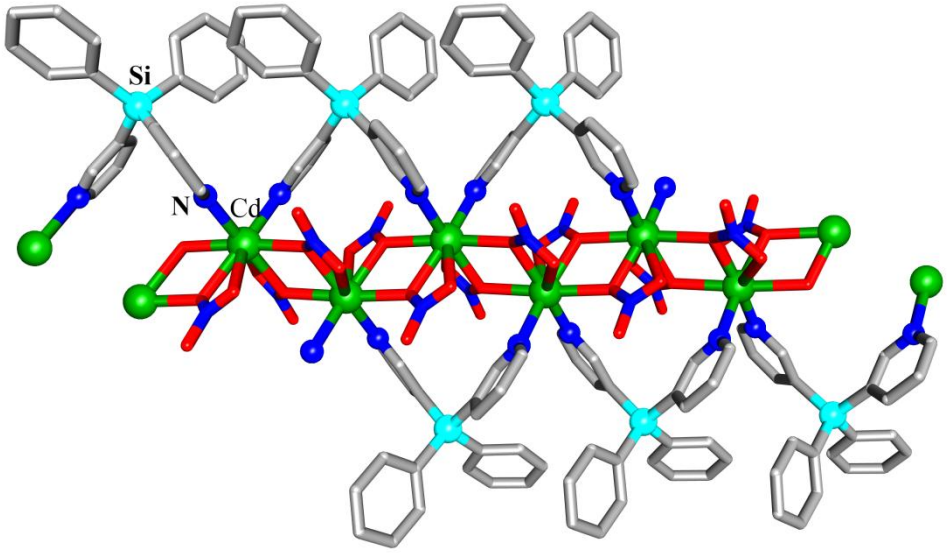

Figure 15: View of one-dimensional network of compound **3.**

3.6 Crystal Structure of Compound 4

Treatment of L^3 with $Cd(NO_3)_2.4H_2O$ gave the compound **4** of formula $[C_{24}H_{20}CdN_4O_6Si]$. In this assembly, the interaction of the L^3 with Cd(II) ion primarily generates a one-dimensional framework(Fig.16). The crystal structure of compound **4** was solved in monoclinic centrosymmetric space group *C2/c* with point group "2/m" and point group symmetry "C_{2h}". Each metal-center has an octahedral geometry in which it is connected to five pyridyl groups through nitrogen atom and the other position is coordinated to oxygen atoms of the nitrate anions. It navigates in a one-dimensional fashion for the formation of coordination network. The asymmetric unit of compound **4** contains one Cadmium metal ion with half occupancy. The bond length between Cd(II) ion and nitrogen atom of pyridyl group is 2.34 Å whereas the bond distance between Cd(II) ion and oxygen atom of nitrate anion is 2.73 Å.

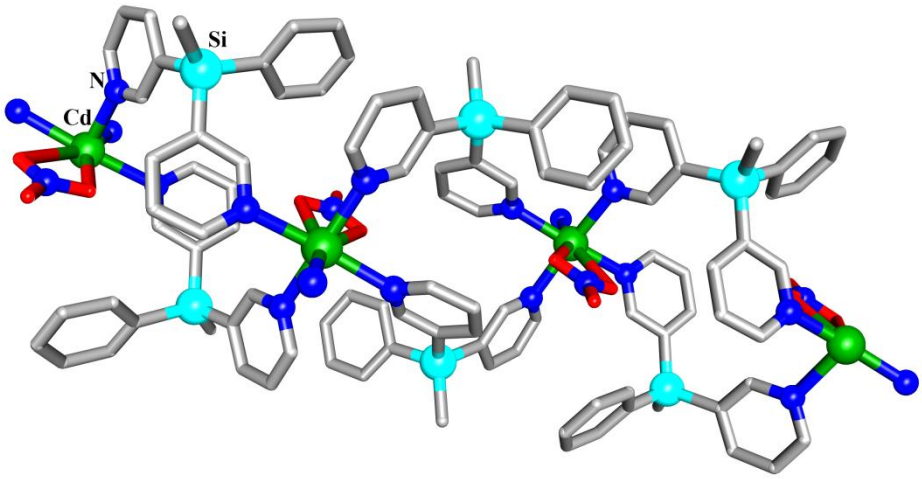

Figure 16: View of one-dimensional network of compound **4**.

3.7 Crystal Structure of Compound 5

Treatment of L^1 with $Co(SCN)_2$ gave the compound 5 of formula $[C_{26}H_{28}CoN_6S_2Si_2]$. The reaction of $Co(SCN)_2$ with L^1 leads to the formation of two-dimensional coordination network (Compound **5**) and its crystal structure was solved in tetragonal non-centrosymmetric space group *P4nc* with point group "4mm" and point group symmetry "C_{4v}". It resulted in the formation of pink crystalline material. In the coordination network, the Co(II) ion has an octahedral geometry in which the four pyridyl groups are attached to it in a planar fashion. The other two positions are occupied by the NCS group in a *trans* geometry. The thiocyanate is a kind of ambidentate ligand which has the ability to coordinate through both Nitrogen as well as Sulfur. However, in compound **5** it is connected to the metal center via the N-donor functionality. Each bis(3-pyridyl)diphenylsilane connects two adjacent cobalt centers and leads to the formation of two-dimensional coordination framework. The bond distances between the Co(II) ion and two nitrogen atoms in the *trans* position are 2.04 Å & 2.06 Å. The two consecutive Co(II) ion center are separated by the Bis(3-pyridyl)diphenylsilane through a distance of 12.92 Å. The Co(II) ion center is connected to the nitrogen of the isothiocyanate in a linear mode such that the angle between Co-N-C is 180°. Since this compound is crystallized in polar non-centrosymmetric space group of tetragonal *P4nc*, we aim to study the ferroelectric behavior of this compound in the future.

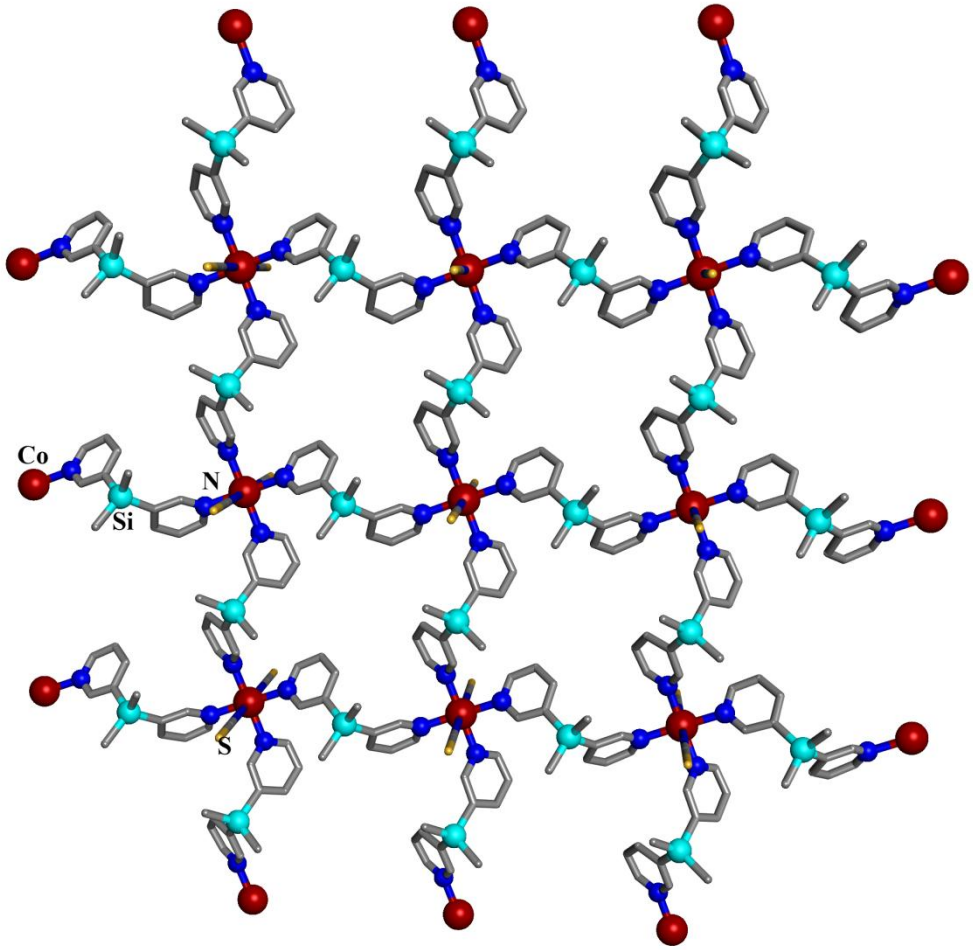

Figure 17: View of the two-dimensional network of compound **5**.

Table1: Space groups of the assemblies derived from dipodal silane ligands with metal salts

Ligand	Metal	Ratio	Formula Unit	Dimensionality of network	Space Group
L^1	$Cd(NO_3)_2.4H_2O$	1:1	$C_{26}H_{28}CdN_4O_6Si$	Two Dimensional	*P4nc* (Non-Centrosymmetric)
L^1	$CdCl_2.H_2O$	1:1	$C_{24}H_{28}CdCl_2N_4Si_2$	Two Dimensional	*P2₁/n* (Centrosymmetric)
L^1	$Co(SCN)_2$	2:1	$C_{26}H_{28}CoN_6S_2Si_2$	Two Dimensional	*P4nc* (Non-Centrosymmetric)

L^2	$Cd(NO_3)_2.4H_2O$	1:1	$C_{22}H_{18}CdN_4O_6Si$	One Dimensional	*P-1* (Centrosymmetric)
L^3	$Cd(NO_3)_2.4H_2O$	1:1	$C_{24}H_{20}CdN_4O_6Si$	One Dimensional	*C2/c* (Centrosymmetric)

For investigating the thermal stability of the compound **1**, Thermo Gravimetric Analysis (TGA) was performed over a range of temperatures from 30°C to 800°C. The TGA plot given in Figure 14 shows that compound **1** is stable up to 175°C, after which it shows an abrupt weight loss implying its decomposition above 175°C. However, melting point for the compound 1 was found to be in the range of 175°C – 200°C from the melting point apparatus.

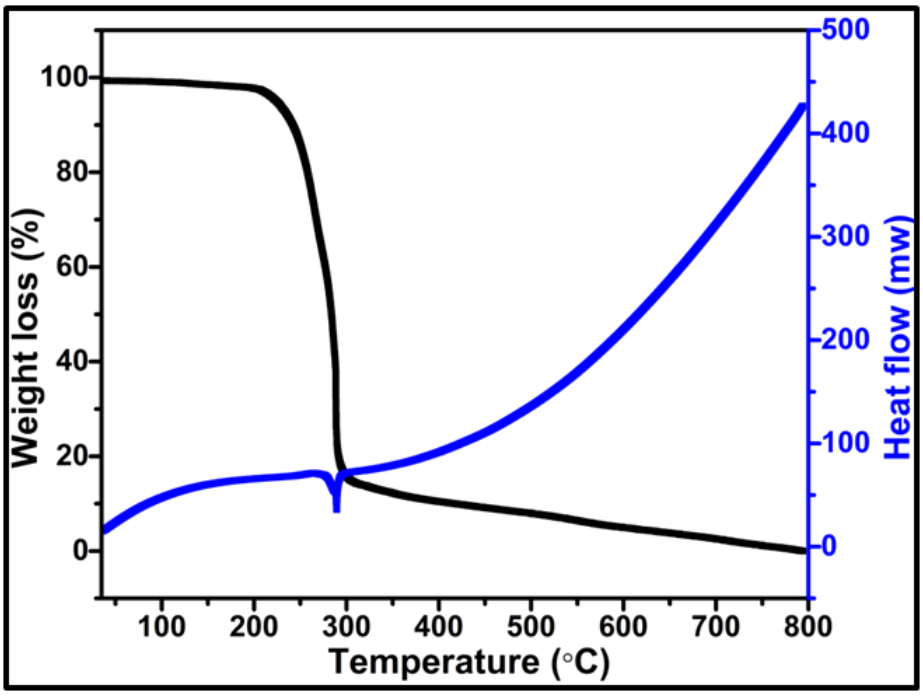

Figure 18: TGA, DTA plot for compound **1**.

3.8 Ferroelectric Studies

To study the ferroelectric behavior, we performed ferroelectric measurements on compound **1**, since it belongs to one of the polar non-centrosymmetric space groups. To study the ferroelectric behavior of compound **1**, we performed ferroelectric

measurements using aixACCT Piezoelectric Evaluation System. Compact disc of diameter 10 mm with 1.31 mm of thickness were made from the powdered samples of compound **1**, which were then electroded using silver adhesive foils.

Ferroelectric Studies at various Temperature with Constant Frequency

Ferroelectric measurements were performed at three different temperatures, i.e., room temperature, 60°C and 100°C at constant frequency of 0.1 Hz (Fig.19). Remarkably, it was observed that maximum remnant polarization of 0.0077 μC/Cm^2 and maximum saturation polarization of 0.0113 μC/Cm^2 were obtained at 100 °C on the application of external electric field.

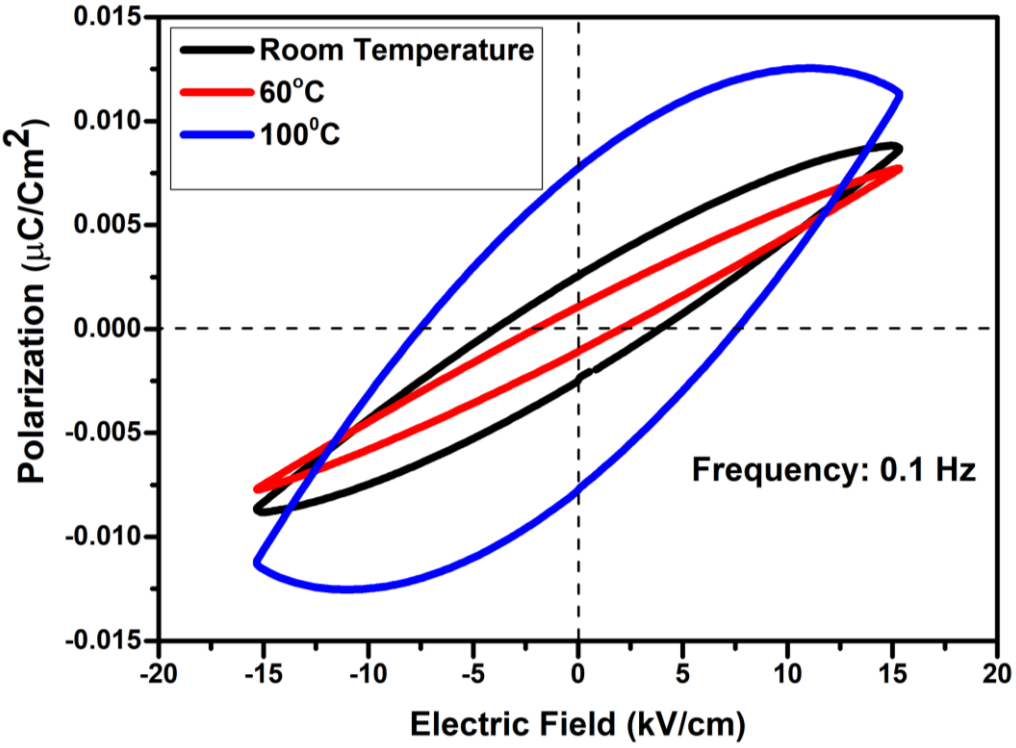

Figure 19: P-E loop at 0.1 Hz at Various Temperatures

Table 2: Values for remnant polarization and saturation polarization at different temperatures.

Temperature (°C)	Remnant Polarization (μC/Cm^2)	Saturation Polarization (μC/Cm^2)
Room Temperature	0.00251	0.0088
60°C	0.00112	0.0077
100°C	0.00779	0.0113

Ferroelectric Studies at Various Frequencies with Constant Temperature

Due to high-temperature stability of compound **1**, ferroelectric hysteresis loops were recorded at 150°C at different frequencies of 5Hz, 10Hz, 20Hz, 50Hz and 100Hz (Fig.20). It was observed that maximum remnant polarization of 0.0162 μC/Cm^2 & maximum saturation polarization of 0.0152 μC/Cm^2 were obtained at 5Hz on the application of external electric field.

Generally, polarization is due to the movement of ions or electrons from the equilibrium position. There are four different types of polarization mechanisms: ionic, electronic, interface and dipolar. In the P-E loop plot (Fig.20), there is decrease in the polarization value for the compound **1** with the increase in the frequency. This trend is due to the fact that, different mass entities have different time scale. The different polarization mechanisms which are ionic, electronic and space charge polarization becomes ineffective at higher frequencies due to higher switching-rate of the electric field which inhibits the dipole to align in the direction of the external electric field.

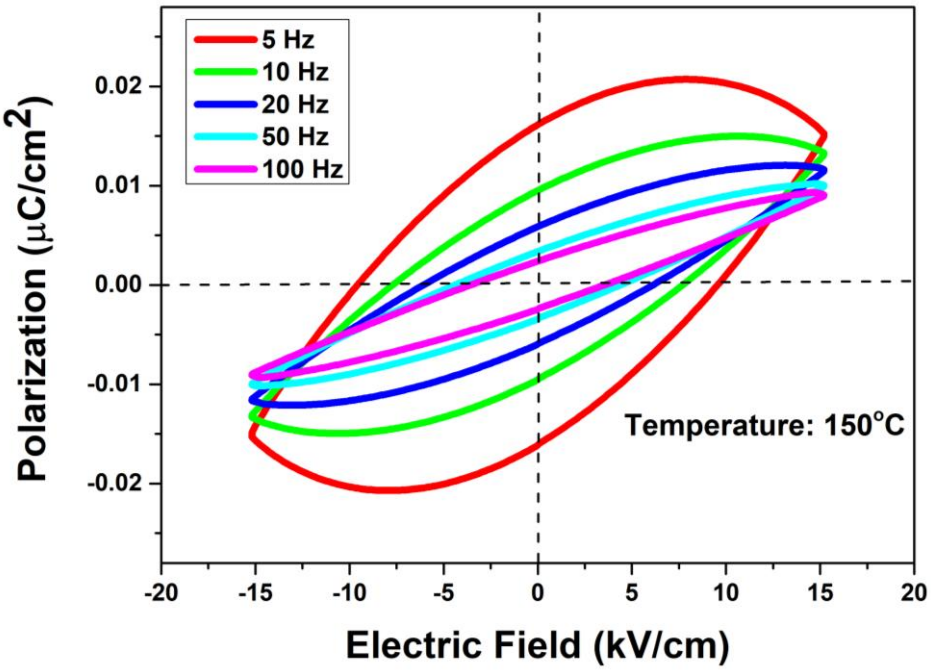

Figure 20: P-E loop with variable frequency at a constant temperature of 150°C.

Table 3 : Values for remnant polarization and sturation polarization at 150°C

Frequency (Hz)	Remnant Polarization (μC/Cm^2)	Saturation Polarization (μC/Cm^2)
5	0.0162	0.0152
10	0.0096	0.0133

20	0.0059	0.0116
50	0.0033	0.0099
100	0.0024	0.0090

Similarly, ferroelectric measurements were also performed at 175°C at two different frequencies of 50Hz and 100Hz. It was observed that maximum remnant polarization of 0.0118 μC/Cm^2 was obtained at 50Hz whereas maximum saturation polarization of 0.0130 μC/Cm^2 was obtained at 100Hz (Fig.21). Although the obtained polarization values are too low, the shapes of the loops and trends in the magnitude polarizations and coercive fields confirm the ferroelectric origin of the obtained loops. These observations also promises the efficacy of utilizing the dipodal silane-based ligands for obtaining metal-organic ferroelectric materials with suitable polarization values.

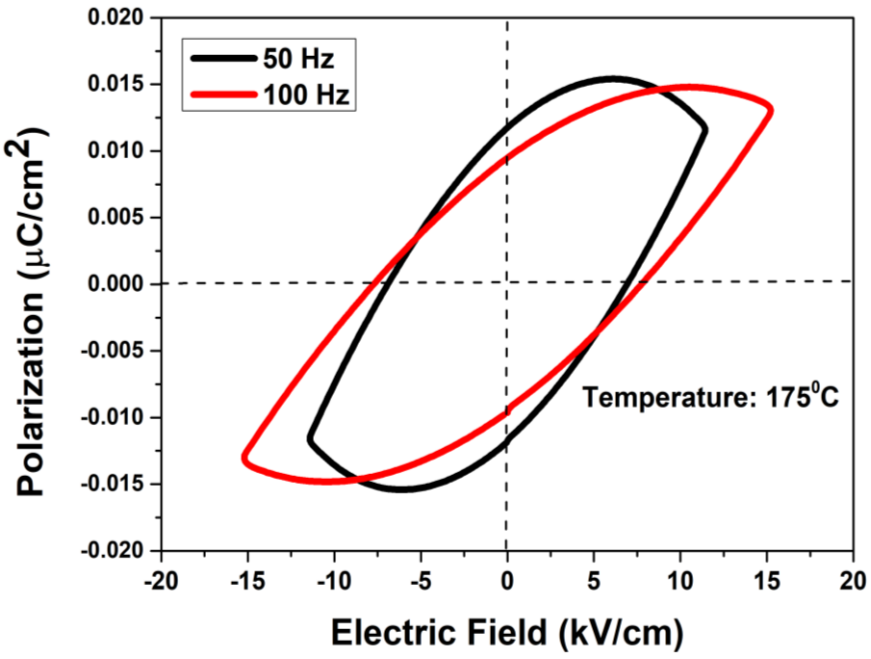

Figure 21: P-E loop with variable frequency at a constant temperature of 175°C

Table 3 : Values for remnant polarization and sturation polarization at 175°C

Frequency (Hz)	Remnant Polarization ($\mu C/Cm^2$)	Saturation Polarization ($\mu C/Cm^2$)
50 Hz	0.0118	0.0116
100 Hz	0.0095	0.0130

3.9 Coordination networks derived from pyridyl functionalized tetrapodal silane ligands

In addition to dipodal silane ligands and their metal complexes, we have also synthesized pyridyl functionalized tetrapodal silane ligand of formula $C_{28}H_{24}N_4Si$ for obtaining interesting examples of coordination materials. The tetrapyridyl tetrasilane ligand L^4 was prepared according to our previously published procedure.[27] By employing the ligand tetrakis(3-pyridyl)vinylsilane in combination with biphenyldicarboxylate (BPDC) linkers and $Zn(NO_3).6H_2O$ (scheme 2) gave rise to an interesting three-dimensional framework Compound **6** of formula $[C_{56}H_{44}Zn\ N_4O_8Si]$.

Scheme 2:

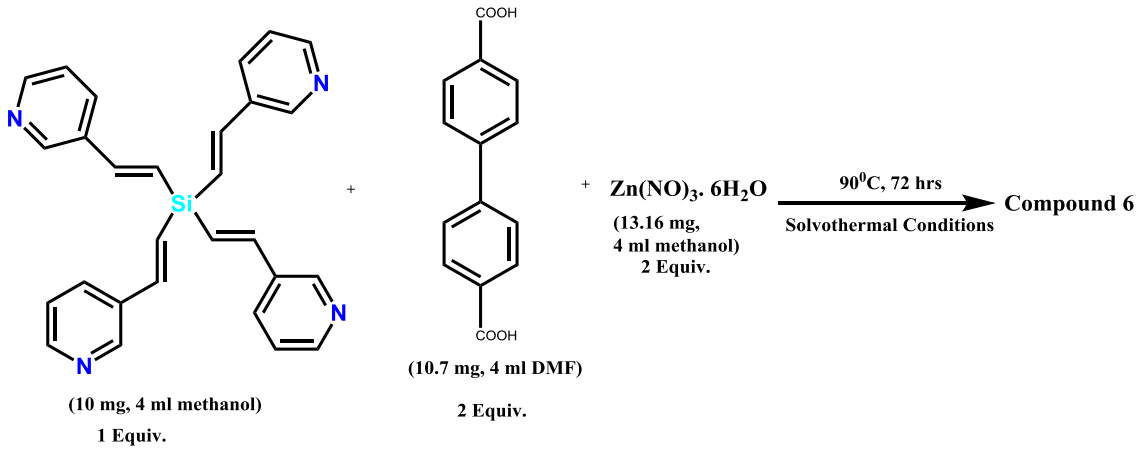

The compound **6** was derived from pyridyl functionalized tetrapodal silane ligand, tetrakis(3-pyridyl)vinylsilane. Its crystal structure was solved in monoclinic centrosymmetric space group *P2₁/n* (Fig.22) with point group "2/m" and point group symmetry "C_{2h}". In this framework, Zn (II) ion adopts an octahedral geometry in which interaction of Zn (II) ions with oxygen atoms of the carboxylic group gives a planar two-dimensional structure. However, the *trans* positions are linked by the pyridyl groups of the tetrapodal silane ligand which leads to the formation of three-dimensional framework.

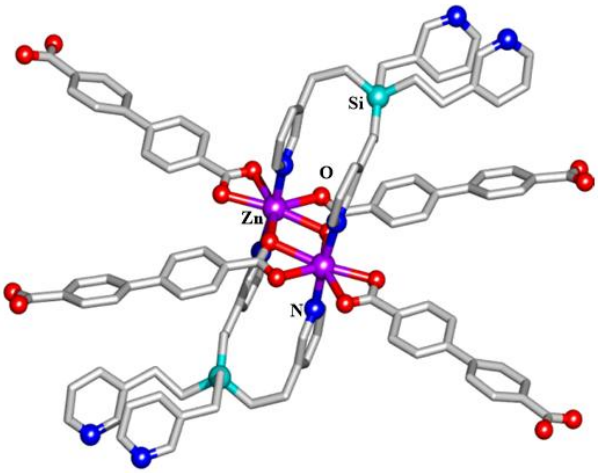

Figure 22: View of three-dimensional network of Compound **6**

However, we are currently working on the further characterization of this compound **6** and its utility in catalysis and gas adsorption.

3.10 Future Aspects

In future, we will be focusing on studying the ferroelectric properties of compound **5**. We would also be studying the dielectric properties for both compound **1** and compound **5** to further understand the polarization attributes of these compounds. Metallation studies of L4 with other metal ions and various other auxiliary carboxylate ligands will also be tested in future with the view of obtaining multi-functional metal-organic frameworks.

Chapter 4

Conclusion

In conclusion, a series of pyridyl functionalized dipodal silane ligands with tetrahedral geometry at the silicon centre were prepared. These ligands were judiciously selected with the view of imparting asymmetry to the metal-complexes coordinated to them. However, only one among the reported metal complexes was found to be crystallized in polar non-centrosymmetric space group (Compound **1**) which was used for ferroelectric studies. The compound **1** exhibited a good ferroelectric hysteresis loop upto 175°C which could be useful for high-temperature ferroelectric applications. The ligand L^1 can be considered as a promising ligand for attaining coordination networks with non-centrosymmetric space group which can be used for designing metal-organic ferroelectric materials. In future, we will be studying the dielectric studies for compound **1** and ferroelectric studies for compound **5** and develop some metal-complexes derived from pyridyl functionalized tetrapodal silane ligands that can be useful for adsorption and catalytic properties.

References

1. Bureekaew, S.; Shimomura, S.; Kitagawa, S. *Sci. Technol. Adv. Mater.* **2008,** 014108.
2. Eddaoudi, M.; Moler, D. B.; Li, H.; Chen, B.; Reineke, T.; O'Keeffe, M.; Yaghi, O.M. *Acc. Chem. Res.* **2001,** 34, 319.
3. Rani, N.; Rao, G.K.; Singh, A. K. *Journ. of Organomet. Chem.* **2009**, 694, 2442–2447.
4. Na, Y. M.; Noh, T. H.; Chun, I. S.; Lee, Y. A.; Hong, J.; Jung, O.S. *Inorg. Chem*. **2008**, 47, 1391-1396.
5. Kim, C. R.; Kang, H.J.; Kim, C. W.; Yoo, K. H.; Jung. O. S. *Trans. Met. Chem.* **2009,** 34, 579-584.
6. Cheetham, A. K.; Rao, C. N. R. *Science* **2007**, 318, 58−59.
7. Whatmore, R. *Springer: New York*, **2007;** pp 597− 623.
8. Cheong, S. W.; Mostovoy, M. *Nat. Mater*. **2007**, 6, 13−20.
9. Ramesh, R. *Nature* **2009**, 461, 1218−1219.
10. Ramesh, R.; Spaldin, N. A. *Nat. Mater*. **2007**, 6, 21−29.
11. Eerenstein, W.; Mathur, N. D.; Scott, J. F. *Nature* **2006**, 442, 759−765.
12. Spaldin, N. A.; Fiebig, M. *Science* **2005**, 309, 391−392.
13. Fu, D.-W.; Cai, H.-L.; Liu, Y.; Ye, Q.; Zhang, W.; Zhang, Y.; Chen, X.-Y.; Giovannetti, G.; Capone, M.; Li, J.; Xiong, R.-G. *Cryst. Sci.* **2013**, 339, 425−428.
14. Horiuchi, S.; Ishii, F.; Kumai, R.; Okimoto, Y.; Tachibana, H.; Nagaosa, N.; Tokura, Y. *Nat. Mater*. **2005**, 4, 163−166.
15. Horiuchi, S.; Tokura, Y. Organic ferroelectrics. *Nat. Mater*. **2008**, 7, 357−366.
16. Jain, P.; Dalal, N. S.; Toby, B. H.; Kroto, H. W.; Cheetham, A. K. *J. Am. Chem. Soc*. **2008**, 130, 10450−10451.
17. Tayi, A. S.; Shveyd, A. K.; Sue, A. C.-H.; Szarko, J. M.; Rolczynski, B. S.; Cao, D.; Kennedy, T. J.; Sarjeant, A. A.; Stern, C. L.; Paxton, W. F.; Wu, W.; Dey, S. K.; Fahrenbach, A. C.; Guest, J. R.; Mohseni, H.; Chen, L. X.; Wang, K. L.; Stoddart, J. F.; Stupp, S. I. *Nature* **2012**, 488, 485−489.
18. Xu, G.-C.; Ma, X.-M.; Zhang, L.; Wang, Z.-M.; Gao, *J. Am. Chem. Soc*. **2010**, 132, 9588−9590.
19. Ye, H.-Y.; Fu, D.-W.; Zhang, Y.; Zhang, W.; Xiong, R.-G.; Huang, S. D. *J. Am. Chem. Soc*. **2009**, 131, 42−43
20. Hang, T.; Zhang, W.; Ye, H.Y.; Xiong, R.-G. *Chem. Soc. Rev*. **2011**, 40, 3577−3598.
21. Valasek, J. *Phys. Rev.* **1921**, *17*, 475-481.
22. Pan, Q.; Liu, Z.-B.; Tang, Y.-Y.; Li, P.-F.; Ma, R.-W.; Wei, R.-Y.; Zhang, Y.; You, Y.-M.; Ye, H.-Y.; Xiong, R.-G. *J. Am. Chem. Soc.* **2017**, *139*, 3954.
23. Zhang, Y.; Liao, W.-Q.; Fu, D.-W.; Ye, H.-Y.; Liu, C.-M.; Chen, Z.-N.; Xiong, R.-G. *Adv. Mater.* **2015**, *27*, 3942.

24. Zhang, Y.; Liao, W. Q.; Fu, D. W.; Ye, H. Y.; Chen, Z. N.; Xiong, R. G. *J. Am. Chem. Soc.* **2015**, *137*,4928.
25. Ye, H. Y.; Zhou, Q.; Niu, X.; Liao, W. Q.; Fu, D. W.; Zhang, Y.; You, Y. M.; Wang, J.; Chen, Z. N.; Xiong, R. G. *J. Am. Chem. Soc.* **2015**, *137*, 13148.
26. Noh, T. H.; Kim, J. H.; Lee, Y. A.; Suh, H.; Jung, O. S. *Journ. of Mol. Struc.* **2004**, 691, 165–169.
27. Deshmukh, M. S.; Chaudhary, A.; Zolotarev, P. N.; Ramamoorthy, B. *Inorg. Chem*. **2017**, 56, 11762−11767.